
This is an electronic reprint of the original article.
This reprint may differ from the original in pagination and typographic detail.

Shalygin, V. A.; Moldavskaya, M. D.; Vinnichenko, M. Ya; Maremyanin, K. V.; Artemyev, A. A.; Panevin, V. Yu; Vorobjev, L. E.; Firsov, D. A.; Korotyeyev, V. V.; Sakharov, A. V.; Zavarin, E. E.; Arteev, D. S.; Lundin, W. V.; Tsatsulnikov, A. F.; Suihkonen, S.; Kauppinen, C.

Selective terahertz emission due to electrically excited 2D plasmons in AlGaIn/GaN heterostructure

Published in:
Journal of Applied Physics

DOI:
[10.1063/1.5118771](https://doi.org/10.1063/1.5118771)

Published: 14/11/2019

Document Version
Publisher's PDF, also known as Version of record

Please cite the original version:

Shalygin, V. A., Moldavskaya, M. D., Vinnichenko, M. Y., Maremyanin, K. V., Artemyev, A. A., Panevin, V. Y., Vorobjev, L. E., Firsov, D. A., Korotyeyev, V. V., Sakharov, A. V., Zavarin, E. E., Arteev, D. S., Lundin, W. V., Tsatsulnikov, A. F., Suihkonen, S., & Kauppinen, C. (2019). Selective terahertz emission due to electrically excited 2D plasmons in AlGaIn/GaN heterostructure. *Journal of Applied Physics*, 126(18), Article 183104. <https://doi.org/10.1063/1.5118771>

This material is protected by copyright and other intellectual property rights, and duplication or sale of all or part of any of the repository collections is not permitted, except that material may be duplicated by you for your research use or educational purposes in electronic or print form. You must obtain permission for any other use. Electronic or print copies may not be offered, whether for sale or otherwise to anyone who is not an authorised user.

Selective terahertz emission due to electrically excited 2D plasmons in AlGaN/GaN heterostructure

Cite as: J. Appl. Phys. **126**, 183104 (2019); <https://doi.org/10.1063/1.5118771>

Submitted: 04 July 2019 . Accepted: 28 October 2019 . Published Online: 13 November 2019

V. A. Shalygin , M. D. Moldavskaya, M. Ya. Vinnichenko, K. V. Maremyanin, A. A. Artemyev, V. Yu. Panevin, L. E. Vorobjev, D. A. Firsov, V. V. Korotyeyev , A. V. Sakharov, E. E. Zavarin, D. S. Arteev, W. V. Lundin, A. F. Tsatsulnikov, S. Suihkonen, and C. Kauppinen 



View Online



Export Citation



CrossMark

ARTICLES YOU MAY BE INTERESTED IN

[Evidence of trap-assisted Auger recombination in low radiative efficiency MBE-grown III-nitride LEDs](#)

Journal of Applied Physics **126**, 184502 (2019); <https://doi.org/10.1063/1.5096773>

[Gallium arsenide x-ray photodiodes for ultrafast physics applications](#)

Scilight **2019**, 461104 (2019); <https://doi.org/10.1063/10.0000261>

[Electron drift velocity in wurtzite ZnO at high electric fields: Experiment and simulation](#)

Journal of Applied Physics **126**, 185703 (2019); <https://doi.org/10.1063/1.5100078>

Lock-in Amplifiers

... and more, from DC to 600 MHz



Selective terahertz emission due to electrically excited 2D plasmons in AlGa_N/Ga_N heterostructure

Cite as: J. Appl. Phys. **126**, 183104 (2019); doi: [10.1063/1.5118771](https://doi.org/10.1063/1.5118771)

Submitted: 4 July 2019 · Accepted: 28 October 2019 ·

Published Online: 13 November 2019



V. A. Shalygin,^{1,a)} M. D. Moldavskaya,¹ M. Ya. Vinnichenko,¹ K. V. Maremyanin,² A. A. Artemyev,¹ V. Yu. Panevin,¹ L. E. Vorobjev,¹ D. A. Firsov,¹ V. V. Korotyeyev,³ A. V. Sakharov,⁴ E. E. Zavarin,⁴ D. S. Arteev,⁴ W. V. Lundin,⁴ A. F. Tsatsulnikov,⁵ S. Suihkonen,⁶ and C. Kauppinen⁶

AFFILIATIONS

¹Department of Physics of Semiconductors and Nanoelectronics, Peter the Great St. Petersburg Polytechnic University, 29 Polytechnicheskaya Str., St. Petersburg 195251, Russia

²Institute for Physics of Microstructures of RAS, Nizhny Novgorod 603950, Russia

³Department of Theoretical Physics, Institute of Semiconductor Physics NASU, Kyiv 03028, Ukraine

⁴Ioffe Institute, 26 Polytechnicheskaya Str., St. Petersburg 194021, Russia

⁵Submicron Heterostructures for Microelectronics Research and Engineering Center of RAS, 26 Polytechnicheskaya Str., St. Petersburg 194021, Russia

⁶Department of Electronics and Nanoengineering, Aalto University, P.O. Box 13500, Aalto FI-00076, Finland

^{a)}Electronic mail: shalygin@rphf.spbstu.ru

ABSTRACT

Terahertz radiation emission from an electrically excited AlGa_N/Ga_N heterostructure with a surface metal grating was studied under conditions of two-dimensional (2D) electron heating by the lateral electric field. Intensive peaks related to nonequilibrium 2D plasmons were revealed in the terahertz emission spectra with up to 4 times selective amplification of the radiation emission in the vicinity of 2D plasmon resonance. This selective emission was shown to be frequency-controllable by the grating period. Exact spectral positions of the 2D plasmon resonances were preliminarily experimentally detected with the help of equilibrium transmission spectra measured at various temperatures. The resonance positions are in a satisfactory agreement with the results of theoretical simulation of the transmission spectra performed using a rigorous solution of Maxwell's equations. The effective temperature of hot 2D electrons was determined by means of *I*-*V* characteristics and their analysis using the power balance equation. It was shown that for a given electric field, the effective temperature of nonequilibrium 2D plasmons is close to the hot 2D electron temperature. The work may have applications in Ga_N-based electrically pumped emitters of terahertz radiation.

Published under license by AIP Publishing. <https://doi.org/10.1063/1.5118771>

I. INTRODUCTION

Plasmonics is a rapidly developing field of science and technology. In particular, plasmonics is promising in obtaining terahertz (THz) radiation emission due to two-dimensional (2D) plasmon excitation. A number of works were focused on the study of emitters, based on the excitation of coherent 2D plasmons and providing a broadband THz radiation (see Refs. 1 and 2 and references therein). This effect was observed in AlGa_N/Ga_N HEMT structures with submicrometer gate length,¹ and it has been theoretically interpreted in terms of Dyakonov–Shur instabilities.³ A grating-gate transistor structure with a spatially modulated 2D

electron channel has been proved to be more effective compared with the single-solid-gate field-effect transistor with 2D electron channel.⁴ An advanced solution is the use of doubly interdigitated grating gates, which was realized on the base of the InGaP/InGaAs/GaAs material system.²

The incoherent mechanism of 2D plasmon excitation in grating-based plasmonic structures was also investigated. Experiments with the incoherent 2D plasmons were carried out on silicon MOSFETs⁵ and AlGaAs/GaAs heterojunctions^{6,7} under conditions of 2D electron heating in a lateral electric field. In the THz electroluminescence spectra, rather narrow peaks associated with the radiative decay of

nonequilibrium 2D plasmons were revealed. The selective THz emission properties of these structures were provided by metal grating at their surface. It has been shown that the THz radiation intensity in the spectral range of the 2D plasmon peak can significantly exceed the radiation intensity from hot 2D electrons with the same effective temperature.^{6,7}

Radiation emission mechanisms associated with the intersubband and multisubband plasmons were investigated in nanostructures based on the AlInAs/InGaAs platform.^{8–10} It was experimentally demonstrated that incorporation of the nanostructures into sub-wavelength microcavity can lead to ultrastrong light-matter coupling when the lower-polariton state lies in the THz region.¹⁰ By injecting a lateral electric current in the quantum well, the authors observed THz emission up to room temperature.

In comparison with above-mentioned AlGaAs/GaAs and AlInAs/InGaAs structures, a higher degree of disequilibrium under electrical excitation can be achieved in AlGaN/GaN heterostructures due to higher electrical strength and temperature stability of the III-nitrides. Therefore, the nitride-based structures are promising for creating THz emitters with electrical pumping. In particular, small footprint THz emitters would enable new possibilities in environmental and chemical sensing. The miniaturized THz emitters could also enable lab-on-a-chip applications¹¹ and new medical diagnostics¹² that for now rely on far bulkier emitters. The promise of using AlGaN/GaN nanostructures to create terahertz emitters based on nonequilibrium 2D plasmons is indirectly indicated by the results of experimental and theoretical studies carried out in Refs. 13–15. Particularly, the interaction of THz radiation with equilibrium 2D plasmons was experimentally studied in the AlGaN/GaN heterostructure, and intensive peaks corresponding to 2D plasmon resonances have been observed in the absorption spectra.¹³

A recent paper¹⁶ was aimed at investigating the selective THz radiation from a AlGaN/GaN heterostructure under electrical excitation of incoherent 2D plasmons. However, only a weak peak related to 2D plasmon scattering at a surface metal grating was detected in the THz emission spectrum. The peak amplitude did not exceed 20% of the wideband background signal caused by significant Joule heating of the whole sample during the applied voltage pulse. The reason for this was the use of very long electrical pulses (800–2000 μ s).

The main goal of the present work is to obtain intensive selective THz emission related to 2D plasmons under essentially nonequilibrium conditions when the effective temperatures of 2D electrons and 2D plasmons are much higher than the lattice temperature. Results of preliminary experimental studies of the optical properties related to 2D plasmons in the AlGaN/GaN heterostructures were partially reported in our recent conference paper.¹⁷ The structure of the present paper is as follows. In Sec. II, spectra of THz transmission and absorption for a GaN/AlGaN heterostructure grown on a sapphire substrate with surface metal gratings of different periods are considered theoretically. On the basis of the simulated spectra, the heterostructure is designed to ensure the maximum amplitude of the fundamental 2D plasmon mode under the condition of a spectral overlap of this mode with the sensitivity range of the chosen THz detector (Ge:Ga). In Sec. III, we describe the heterostructure growth process, postgrowth device fabrication

(including contact and grating fabrication), geometry of the samples, and results on the 2D electron gas (2DEG) characterization. In Sec. IV, we examine the equilibrium optical transmission spectra of the samples with different grating periods and reveal 2D plasmon resonances. In Sec. V, current-voltage characteristics for the samples with a metal grating and without it are analyzed using the power balance equation. This analysis allows us to determine a field dependence of the hot 2DEG temperature. Finally, in Sec. VI, we discuss experiments on THz electroluminescence under 2D electron heating in a pulsed electric field. We used a fast Ge:Ga detector, which enables the use of short voltage pulses ($\sim 2 \mu$ s) to provide a weak Joule heating of the sample during the pulse. This made it possible to observe intensive peaks of THz radiation corresponding to 2D plasmon resonance. For the AlGaN/GaN material system, it has been done for the first time.

II. MODELING OF EQUILIBRIUM TRANSMISSION AND ABSORPTION SPECTRA

To optimize the design of the structure purposed for investigation of THz emission related to grating-coupled 2D plasmons, we first performed the theoretical modeling of equilibrium transmission and absorption spectra for an AlGaN/GaN heterostructure with a surface metal grating. We considered the normal incidence of radiation and found a rigorous solution of Maxwell's equations applying the integral equation technique and the Galerkin scheme,^{18,19} which give fast convergence and controlled accuracy of computations. Calculations were carried out for a temperature $T = 77$ K.

Simulated transmittance spectra for the radiation with the electric field vector perpendicular to metal strips of the grating (p -polarization) demonstrate a sequence of dips corresponding to excitation of different 2D plasmon modes. Simultaneously, one can observe a set of peaks at the same spectral positions in simulated absorptivity spectra for p -polarized radiation. A dip (peak) with the lowest frequency corresponds to the fundamental 2D plasmon mode with the wavevector $q = 2\pi/a$, where a is the grating period.

The shift of the plasmon resonances under variation of the grating period relates to fundamental properties of the 2D plasmons, which have a square-root dispersion relation for unscreened 2DEG and a linear dispersion for the case of screened 2DEG. In the plasmonic structures with a surface metal grating, the positions of 2D plasmon resonances are located between the resonance frequencies for the screened and unscreened plasmons (see Refs. 6, 7, and 20). In particular, for the fundamental 2D plasmon mode, the resonance frequency for a grating-based plasmonic structure in a case of small/large grating filling factor can be estimated using the plasmon frequency of unscreened/screened plasmons calculated at the wavevector $q = 2\pi/a$. It means that if we decrease a grating period keeping the same filling factor, the resonance frequency should increase. The latter is true for any 2D plasmon order (in particular, for the fundamental mode) for an arbitrary filling factor and was approved by rigorous electrodynamic simulation (see Fig. 1) and by the transmittance measurements (see Sec. IV).

We set out to design and fabricate structures providing maximum amplitude of the fundamental 2D plasmon mode under the condition of a significant spectral overlap of this mode with the

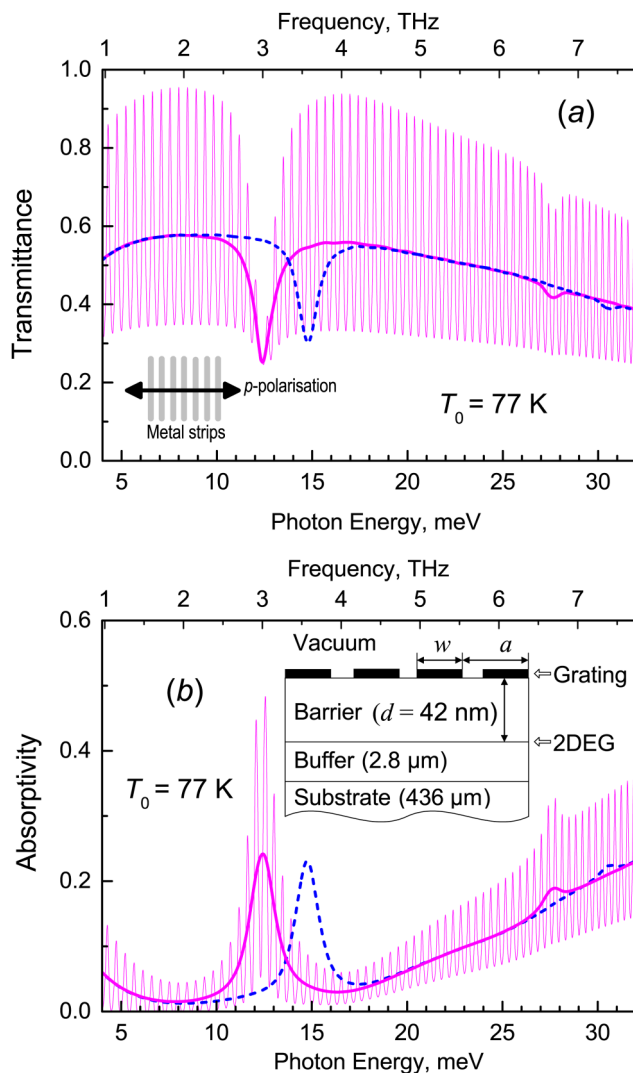


FIG. 1. Simulated transmittance (a) and absorptivity (b) spectra of the structures with different grating geometries for the radiation with p -polarization. Thin solid lines represent the results of simulation for ideal monochromatic radiation for the grating period $a = 1000$ nm, and metal stripe width $w = 500$ nm. Thick solid lines show the results of the averaging of the thin curves with respect to a period of Fabry–Pérot oscillations. Dashed lines represent the simulation results after the spectral averaging for the 800-nm-period grating with $w = 400$ nm. Arrow in the inset in panel (a) shows the direction of the electric field oscillations for p -polarized radiation (in respect to the metal strips of the grating). Inset in panel (b) demonstrates a cross section of the structure.

sensitivity range of the Ge:Ga detector (9–26 meV at the level of 20%). To choose an appropriate design, four parameters varied in the spectra simulation, namely, 2D electron concentration n_s , distance between 2D electron channel and metal grating d (i.e., the thickness of the AlGaIn barrier layer), grating period a and metal strip width w . Thicknesses of the sapphire substrate and GaN

buffer layer were fixed at typical values (436 μm and 2.8 μm , respectively). The frequency dispersion of the dielectric permittivity of the sapphire in the considered spectral range was taken from our experimental data, which will be published elsewhere. The barrier and buffer layers were assumed dispersionless with static dielectric permittivities of 9.4 and 8.9, respectively. The optical properties of 2DEG were described by the standard Drude–Lorentz model. We considered a δ -thick gold grating with effective 2D conductivity of 2.4×10^{12} cm/s, which corresponded to bulk conductivity of the gold 4×10^{17} s $^{-1}$ and a thickness of the gold strips of 60 nm.

In accordance with calculations, high-frequency shift (blue-shift) of the fundamental 2D plasmon mode can be achieved by four ways: (i) increase of the concentration n_s , (ii) increase of the distance d , (iii) decrease of the period a , and (iv) decrease of the filling factor w/a . Besides, it should be noted that amplitudes of 2D plasmon resonances increase with increasing 2D electron mobility but decrease with increasing the distance d and/or decreasing the filling factor w/a .

Analysis of the calculated spectra showed that the maximum amplitude of the fundamental mode in the chosen spectral range can be obtained in the AlGaIn/GaN structure with the following parameters: concentration $n_s = 1.2 \times 10^{13}$ cm $^{-2}$, distance $d = 42$ nm, period $a = 1000$ nm, and ratio $w/a = 1/2$. The results of the transmittance and absorptivity spectra simulation for such a structure are shown in Figs. 1(a) and 1(b) by solid lines. The spectra were calculated with 2D electron mobility of 7200 cm 2 /V s. Thin solid lines represent the results of the simulation for ideal monochromatic radiation. In this case, both spectra oscillate over the whole considered spectral range with a short period of 0.3–0.4 meV due to multiple radiation reflections between the structure surface and back of the substrate. To eliminate these interference effects, the spectra were averaged over the period of the Fabry–Pérot oscillations. Resulting spectra are shown in Figs. 1(a) and 1(b) by the thick solid curves. Despite a decrease in the spectral resolution (up to 0.4 meV), 2D plasmon resonances of the first and second order are clearly visible in these curves at photon energies of 12.4 and 27.5 meV, respectively. In the transmittance spectrum, these resonances manifest themselves as dips [Fig. 1(a)], while in the absorptivity spectrum they appear as peaks [Fig. 1(b)]. The monotonic decrease of the transmittance with decreasing photon energies in the spectral range < 8 meV is due to Drude absorption of 2D electrons. The decrease of the transmittance at photon energies exceeding 17 meV is connected with a low-frequency tail of the phonon absorption in the sapphire substrate.²¹ The amplitude of the fundamental 2D plasmon mode in the absorptivity spectrum is rather large (0.24), which is important for studying the THz emission associated with 2D plasmons (according to Kirchhoff's law, at thermal equilibrium the emissivity is equal to the absorptivity).

It should be noted that the obtained spectral position of the fundamental 2D plasmon mode is located in the interval between $\hbar\omega_s = 10.1$ meV and $\hbar\omega_{us} = 21.7$ meV, where $\hbar\omega_s$ and $\hbar\omega_{us}$ are energies of the screened and unscreened 2D plasmons calculated for the wavevector of $2\pi/a$ using corresponding dispersion dependencies (see Refs. 6, 7, and 20).

We examined the transformation of simulated transmission and absorptivity spectra with a change in the period of the metal

grating. It was shown that with a decrease in the grating period to 800 nm, the fundamental 2D plasmon mode undergoes a noticeable high-frequency shift (~ 2.3 meV) but remains within the sensitivity range of the Ge:Ga detector. At the same time, the amplitude of the mode decreases only slightly [see Fig. 1(b)]. This is a most encouraging modeling outcome as it points to the possibility of fabricating terahertz emitters in which operating frequency is controlled by the grating period.

Similar calculations were also carried out for the radiation with the electric field vector parallel to metal strips of the grating (*s*-polarization). In this case, over the whole considered spectral range, the reflectivity of the structure exceeds 0.99 but transmittance and absorptivity (emissivity) are close to zero. These features are entirely due to the metal grating. Two-dimensional electrons and plasmons in the AlGaIn/GaN structure have practically no effect on the spectra for *s*-polarized radiation. This is why experimental studies in this work were performed exclusively with *p*-polarized radiation.

III. HETEROSTRUCTURE GROWTH AND POSTGROWTH DEVICE FABRICATION

The investigated epitaxial AlGaIn/GaN 2DEG heterostructures were grown by the metalorganic chemical vapor deposition (MOCVD) method on *c*-plane sapphire substrates with a thickness of $436\ \mu\text{m}$. Growth was performed using standard precursors: trimethylgallium, trimethylaluminum, ammonia, and silane. Details of the growth procedure were published elsewhere.²² The heterostructure consisted of an undoped insulating 2800-nm-thick GaN buffer layer, an ~ 0.7 -nm-thick AlN interface layer, a 35-nm-thick AlGaIn barrier layer, a 4-nm-thick GaN cap layer, and was covered by a 2.5-nm-thick *in situ* deposited amorphous Si_3N_4 dielectric. For stable operation of ohmic contacts at low temperatures, the upper part (23 nm) of the AlGaIn barrier and entire GaN cap layer were *n*-doped by Si with a concentration about of $5 \times 10^{18}\ \text{cm}^{-3}$. A total distance from the 2DEG channel at the GaN/AlN interface to the heterostructure surface was about 42 nm. The 2D electron concentration, deduced from the Hall effect and conductivity measurements by the Van der Pauw method, was $n_s = (1.15 \pm 0.05) \times 10^{13}\ \text{cm}^{-2}$ with the low-field mobility $\mu_0 = 7000\text{--}7700\ \text{cm}^2/(\text{V s})$ at the temperature of 77 K.

To apply a lateral electric field to 2DEG, the electrical contacts were patterned by photolithography. First, standard Ti/Al/Ni/Au (40/30/30/40 nm) metal stacks were formed. Every sample had two contact pads ($4.5 \times 1.5\ \text{mm}^2$) at a distance of 3.5 mm from each other. Second, additional Ni/Au (25/25 nm) stacks of a smaller size were patterned above the contact pads. The contacts showed Ohmic behavior, and contact resistance values measured at the temperatures of 4.2–77 K were in the range of 12–18 Ω .

A metal grating on the sample surface was formed via electron beam lithography. For metallization, Ti/Au (5/60 nm) stacks were evaporated. The grating was located in the region between contacts. It was made rather large ($4.5 \times 3\ \text{mm}^2$) to have a sufficient area for THz emission gathering. Samples with two different grating periods were fabricated: $a = 801 \pm 5$ and 1010 ± 8 nm. A filling factor of these gratings was $w/a = 0.498 \pm 0.009$ and 0.489 ± 0.004 , respectively. These parameters were determined using scanning

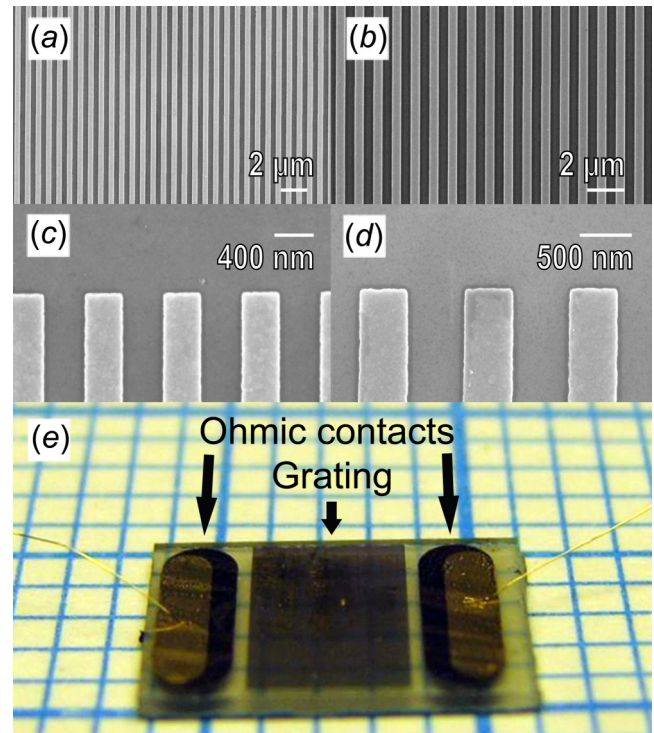


FIG. 2. SEM images of the metal gratings with the periods of 801 nm [(a) and (c)] and 1010 nm [(b) and (d)]. Photo of a single grating sample (e); on the graph paper in the background, each small square is 1 mm wide.

electron microscopy (SEM) images of a few different parts of the gratings. Very small standard deviations of the measured parameters over the grating area indicate a high homogeneity of the fabricated metal gratings. Typical SEM images of the gratings are presented in Figs. 2(a)–2(d). Panels (c) and (d) show images of the very edge of the metal stripes demonstrating the almost ideal control of the geometry that high-resolution electron beam lithography can offer. After wafer dicing, all the samples had uniform dimensions: $7 \times 5\ \text{mm}^2$ [see Fig. 2(e)]. (For a more detailed description of the postgrowth device fabrication, see the [supplementary material](#).)

IV. EXPERIMENTAL STUDY OF EQUILIBRIUM TRANSMISSION SPECTRA

The equilibrium optical transmission spectra of the AlGaIn/GaN heterostructures were experimentally studied in the THz spectral range using a Fourier spectrometer Bruker Vertex 80v operating in a rapid-scan mode. The spectrometer was evacuated. A globar was used as a source of THz radiation and a Mylar beam-splitter was applied. The sample under investigation was mounted on the cold-finger of a closed cycle cryostat. The intensity of the transmitted THz radiation was measured by a pyroelectric detector. The experimental transmission spectra were recorded

under the normal incidence of radiation. Measurements were carried out in the temperature range $T_0 = 5\text{--}300\text{ K}$.

It has been shown experimentally that it is possible to eliminate the Fabry–Pérot oscillations discussed in Fig. 1 by appropriate choice of the spectral resolution of the spectrometer. A low resolution of about 0.5 meV was chosen (for details, see the supplementary material).

The optical transmittance spectra for the samples with surface metal grating obtained for p -polarized radiation are shown in Fig. 3. The sample with 1010-nm -period grating demonstrates two resonances, namely, a narrow dip at the photon energy of 9.9 meV and a wide dip at 20.8 meV . The spectral half-width of the latter is about 3 times greater than that of the former. When the grating period decreases to 801 nm , the low-frequency dip shifts up by 1.7 meV in photon energy, while the high-frequency dip does not change its spectral position (see Fig. 3). As it was mentioned in Sec. I, the blueshift of the 2D plasmon modes with decreasing grating period is one of the specific features of the grating-based plasmonic structures. Therefore, it can be assumed that the low-frequency dip is associated with 2D plasmons, but the high-frequency dip has another (nonplasmonic) origin. An additional argument in favor of these assumptions is the study of the behavior of both the spectral lines when the temperature changes. In Fig. 4, the transmittance spectra for the sample with 801-nm -period grating are shown at different temperatures. As the temperature rises from 5 to 150 K , the half-width of the low-frequency dip increases from 1.35 ± 0.05 to $1.60 \pm 0.05\text{ meV}$, which correlates

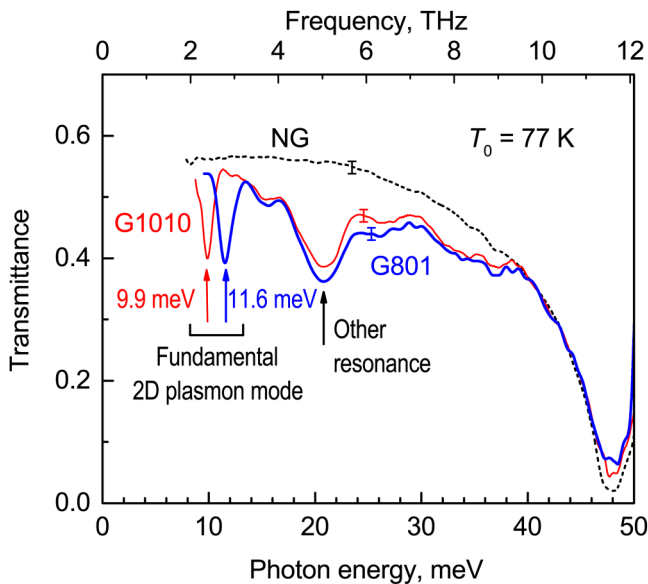


FIG. 3. Optical transmittance spectra of different samples measured at a spectral resolution of 0.5 meV . Labels G1010, G801, and NG mark experimental results for the 1010-nm -period grating, 801-nm -period grating, and no-grating sample, respectively. The transmittance of the grating samples was measured for p -polarized radiation, and transmittance of the reference sample without grating was examined for unpolarized radiation.

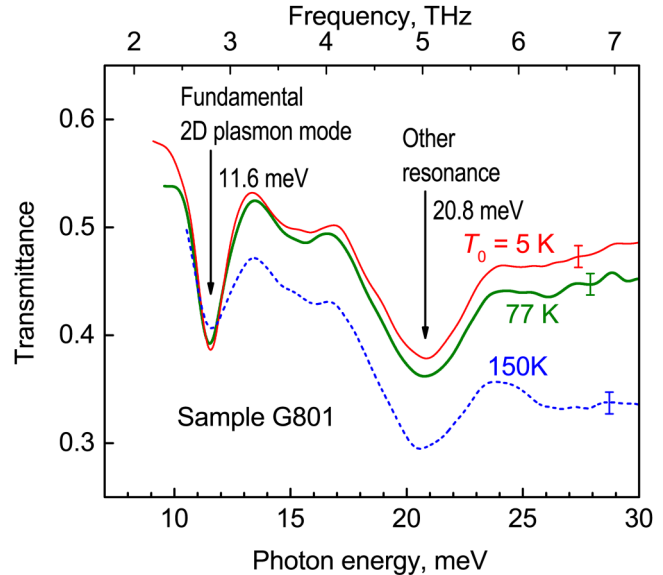


FIG. 4. Optical transmittance spectra for the sample with 801-nm -period grating measured at a spectral resolution of 0.5 meV for different temperatures.

with a decrease in the quality factor of 2D plasmon resonance due to 2D electron mobility falling with temperature [$\mu_0(5\text{ K})/\mu_0(150\text{ K}) = 1.27$]. Note that under these conditions, the half-width of the high-frequency dip remains unchanged ($3.9 \pm 0.1\text{ meV}$). The origin of this resonance is out of scope of the present paper.

As it was mentioned in Sec. III, the grating inhomogeneity degree provided by electron beam lithography was rather low. One can evaluate the 2D plasmon resonance broadening due to small fluctuations of the grating period a and filling factor w/a over the grating area. In accordance with our estimations for the sample with 801-nm -period grating which is characterized by standard deviations $\Delta a = 5\text{ nm}$ and $\Delta(w/a) = 0.009$, the grating inhomogeneity should result in the resonance broadening of $\sim 0.1\text{ meV}$, which is negligibly small compared to the experimentally measured half-width of the 2D plasmon resonance (1.35 meV).

Low-frequency resonance positions in the experimental transmittance spectra (Fig. 3) are close to the theoretically simulated spectral positions of the fundamental 2D plasmon mode for the samples under investigation (Fig. 1). Accordingly, we attribute these experimentally observed resonances as 2D plasmon resonances of the first order. A small divergence between the measured and calculated values of the 2D plasmon mode frequencies may be due to the following reasons. (i) 2D electron concentration in a plasmonic structure can differ from that in a bare structure due to the presence of the metal nearby 2DEG, which can result in a depletion effect. The best fitting of the experimental results was obtained by the simulation with a smaller concentration of $8 \times 10^{12}\text{ cm}^{-2}$. Perhaps, there is an effect of the spatial modulation of 2D electron concentration under the grating. (ii) In the simulation, 2DEG sheet and metal grating were considered as delta-layers,

and their finite thickness was not taken into account. (iii) For simplicity, we considered the multilayer system between 2DEG sheet and grating as a single layer with dielectric permittivity corresponding to the AlGaN barrier layer.

V. DETERMINATION OF HOT 2D ELECTRON TEMPERATURE FROM *I-V* CHARACTERISTICS

Before investigating the THz electroluminescence, we studied the current-voltage characteristics and determined the electric field dependence of the effective temperature of hot 2D electrons. For this purpose, we used methods developed by us earlier.^{23,24} As will be shown below, under certain conditions, an essentially nonequilibrium situation can be realized in AlGaN/GaN heterostructures when the effective temperature of 2D electrons (T_e) is much higher than the lattice temperature (T). These conditions are preferable for the study of terahertz emission due to nonequilibrium 2D plasmons.

To achieve a condition of $T_e \gg T$, we immersed a sample into liquid helium so that in the absence of an electric field, $T_e = T = T_0 = 4.2$ K. Then, we applied pulsed voltage to the sample contacts and chose the duration and repetition rate of the pulses ensuring the condition of $T_e \gg T$ at the end of the pulse. The method for determining the heating degree of the sample lattice $\Delta T = T - T_0$ will be described below in Sec. VI.

Here, we present analysis of the *I-V* characteristics measured in all the samples with *single* voltage pulses of $2 \mu\text{s}$ duration. As it will be shown below in Sec. VI, in such conditions, the ratio $T_e/T \geq 6.6$ under electric fields $E = 50\text{--}450$ V/cm and does not fall below 4 even for the fields up to 2300 V/cm. The electric field dependencies of 2D electron mobilities μ extracted from the *I-V* characteristics (assuming that electron concentration remains constant) are shown in Fig. 5(a). It should be emphasized that in both the grating samples, the dependencies $\mu(E)$ are the same as in the reference sample (within experimental error). Consequently, the surface metal grating in the area between the contacts does not change the strength of the current in 2DEG channel compared with the reference sample.

The experimentally determined dependence $\mu(E)$ allows finding the field dependence of hot 2D electron temperature T_e . It is known that in AlGaN/GaN heterostructures with a 2D electron concentration of $\sim 1 \times 10^{13} \text{ cm}^{-2}$ and more, intense electron-electron collisions ensure the formation of the symmetric part of the distribution function in the electric field in the form of a Fermi-Dirac function with effective temperature T_e ,²³

$$f(\epsilon, T_e) = \frac{1}{\exp((\epsilon - \epsilon_F)/k_B T_e) + 1}, \quad (1)$$

where ϵ_F is the Fermi energy and k_B is the Boltzmann constant. In average, the power which an electron gets from an applied electric field is equal to its energy losses through inelastic scattering processes and can be described by the power balance equation²³⁻²⁵

$$e\mu E^2 = \left\langle \frac{d\epsilon}{dt} \right\rangle, \quad (2)$$

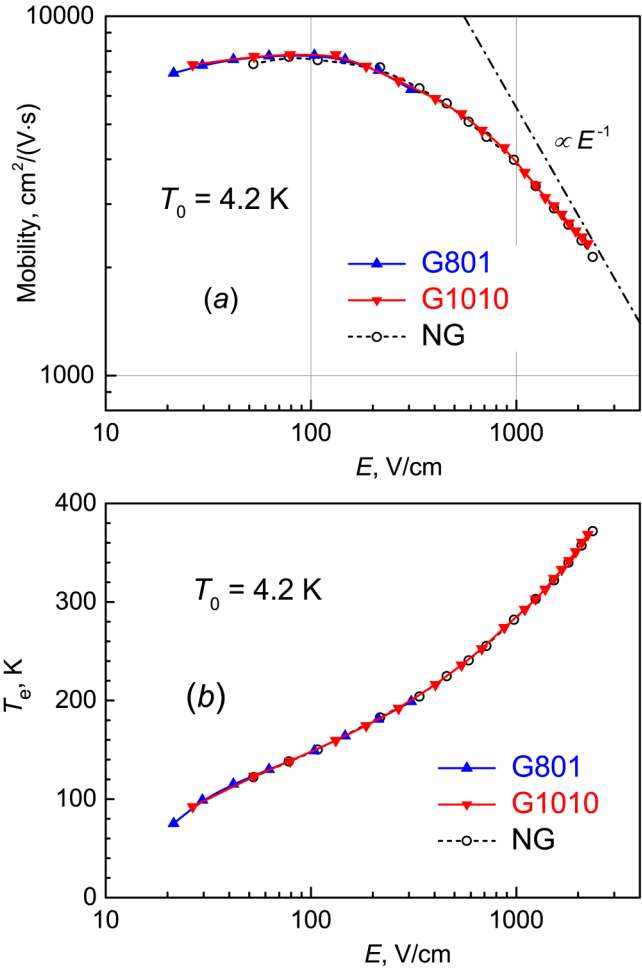


FIG. 5. Field dependencies of 2DEG mobility (a) and effective temperature T_e (b) for different samples. The same sample designations are used as in Fig. 3. The solid and dashed lines in the figure are a guide for the eye. The dashed-dotted line in panel (a) shows a high-field asymptote for the 2D electron mobility corresponding to the drift velocity saturation under conditions of intensive polar optical phonon scattering.

where $\langle \frac{d\epsilon}{dt} \rangle$ is the total energy loss rate per one carrier for all energy scattering mechanisms averaged over the distribution function. Because this function depends on the hot electron temperature T_e , the latter can be easily found using Eq. (2). The algorithm for calculating the total energy loss rate is described in Ref. 23. To solve the power balance equation, we applied the semiempirical method using the dependence $\mu(E)$ from our experiments [Fig. 5(a)]. Calculations lead to the same field dependence of hot 2D electron temperature for all the samples [see Fig. 5(b)]. In particular, in the samples cooled to the temperature of liquid helium, two-dimensional electrons were heated to a temperature $T_e = 370$ K at a pulsed electric field $E = 2300$ V/cm.

VI. EXPERIMENTS ON TERAHERTZ ELECTROLUMINESCENCE

In order to investigate THz electroluminescence, we performed two experiments. In the first one, the integrated intensity of THz radiation was detected by a Ge:Ga detector, and a dependence of the photoresponse on the applied electric field was studied. The second experiment was devoted to spectral studies of the THz electroluminescence using the same detector and a magnetic-field-tuned InSb filter. Both the experiments were conducted on samples with and without metal grating under conditions of significant 2D electron heating.

The sample and entire optical part of the experimental setup including the detector were located inside the Dewar transport vessel filled with liquid helium; thus, undesirable sample illumination with room-temperature background radiation was avoided. A 3 T superconducting solenoid was placed between the sample and the detector. A *n*-InSb plate was mounted at the center of the solenoid. When the magnetic field in solenoid is swept up to 3 T, the spectral position of the cyclotron resonance (CR) in *n*-InSb changes linearly to 27.2 meV. The spectral range covered by the present detection system is limited by the sensitivity range of the Ge:Ga detector, while the spectral resolution is determined by the cyclotron resonance line width (2.2 meV). At the time of the integral photoresponse measurements, the *n*-InSb filter was removed from the solenoid.

To increase the signal-to-noise ratio, we applied periodic voltage pulses to the sample and measured the photoresponse signal using a low-noise current preamplifier and a gated integrator with boxcar averager. Compared with single pulses (see Sec. V), when using periodic pulses, the maximum electric field strength in the sample should be reduced. During the time between pulses, the sample lattice is required to cool to a temperature $T_0 = 4.2$ K, otherwise an increase in this temperature is inevitable, which may be accompanied by boiling of helium and an abrupt decrease in the heat removal rate. For this reason, in electroluminescence studies with a pulse duration of $2\ \mu\text{s}$ and a repetition frequency of 10 Hz, the maximum electric field strength was limited to ~ 500 V/cm.

Electric field dependence of the integral intensity of the THz radiation from different samples is demonstrated in Fig. 6. It is known that THz electroluminescence in AlGaIn/GaN heterostructures without surface metal gratings is associated with thermal radiation of hot 2D electrons²³ and consequently is unpolarized. It is this mechanism of THz radiation emission that occurs in the reference sample. As the electric field increases from 20 to 450 V/cm, the hot electron temperature T_e in the reference sample increases from 60 to 225 K (see Fig. 5). This is accompanied by a magnification in the integral radiation intensity by about two orders of magnitude (see dashed line in Fig. 6). As mentioned above, the same dependence $T_e(E)$ is inherent for the sample with a metal grating. If only this THz emission mechanism took place in the grating sample, then it would give half the integral radiation intensity for a given value of the electric field, since the metal grating transmits waves with only one linear polarization (*p*-polarization) and totally reflects back the waves with orthogonal linear polarization. However, the experiment showed that the metal grating on the sample surface does not cause a decrease in the integral

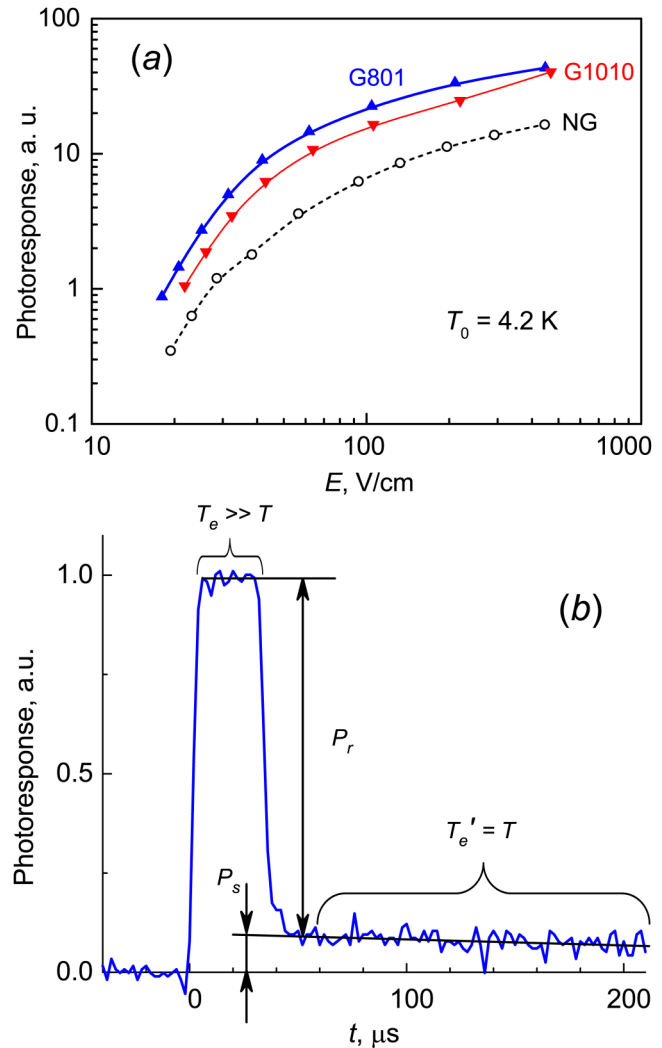


FIG. 6. (a) Field dependence of the integral intensity of the THz radiation from different samples under 2D electron heating in a lateral electric field. Photoresponse was measured by a Ge:Ga detector using periodic $2\text{-}\mu\text{s}$ field pulses with a repetition frequency of 10 Hz. The same sample designations are used as in Figs. 3 and 5. The lines are a guide for the eye. (b) Photoresponse oscillogram for the reference sample without grating (at a single electric field pulse with a duration of $32\ \mu\text{s}$ and $E = 290$ V/cm).

photoresponse signal but, on the contrary, causes it to increase by 3–4 times for the sample with the 801-nm-period grating and by 2–3 times for one with the 1010-nm-period grating (see Fig. 6). This can be explained by an additional contribution to the THz emission due to nonequilibrium 2D plasmons generated during the heating of the electrons by the electric field. According to the results of simulations considered in Sec. II, the 2D plasmon contribution to radiation is expected to be *p*-polarized. As it will be shown below, the THz emission spectrum in each grating sample

demonstrates a resonant peak at the spectral position corresponding to the fundamental 2D plasmon mode. In the sample with the 801-nm-period grating, the integral photoresponse signal is noticeably larger than in the sample with the 1010-nm-period grating. It is due to the fact that in the first case, the 2D plasmon mode (11.6 meV) is close to the maximum sensitivity point of the Ge:Ga detector (~ 13 meV), but in the second case it turns out to be rather far from this point.

Additionally, we studied the photoresponse oscillograms for the reference sample under its excitation by single and periodic pulses of the electric field with various strength (50–450 V/cm) and pulse duration (2–32 μ s). A digital oscilloscope was used for the measurements. Generally, the photoresponse decay can be decomposed into two components. The rapid component of the photoresponse decay [in Fig. 6(b) its amplitude is denoted by P_r] decreases exponentially with time and vanishes in 10 μ s, its duration is determined by the time constant of the Ge:Ga photodetector (~ 2 μ s). The slow component has a much larger duration (up to ~ 100 ms at high fields) and its amplitude (denoted by P_s) increases with increasing the field pulse duration. We assumed that the amplitude of the slow decay component P_s is determined by the Joule heating of the sample lattice during the field pulse. In the considered spectral range, electroluminescence from the reference sample is associated with only one emission mechanism, namely, blackbodylike thermal emission of nonequilibrium 2D electrons. Then, the lattice temperature T corresponding to the very beginning of the slow decay component should be equal to the 2D electron temperature T_e' just after their thermalization ($T_e' = T = T_0 + \Delta T$, where ΔT characterizes the heating degree of the sample lattice). A joint analysis of Figs. 5 and 6 gives a one-to-one relationship between the temperature of the 2D electrons T_e during the field pulse and the amplitude of the rapid photoresponse component P_r . Using this relationship, one can determine $T_e' = T$ corresponding to the amplitude of the slow photoresponse component P_s , and consequently, ΔT .

In oscillograms recorded with single and periodic 2- μ s pulses of $E \leq 450$ V/cm, the slow component of the photoresponse decay is almost indistinguishable ($P_s/P_r < 0.02$). However, it becomes measurable at a single pulse duration of 8 μ s or larger, in particular, in the case of $E = 450$ V/cm (corresponding to $T_e = 223$ K) and a pulse duration of 8 μ s, the ratio $P_s/P_r = 0.10$. Following the above algorithm, we found $\Delta T(8 \mu\text{s}) = 103$ K. This means that with an operating pulse duration of 2 μ s, the lattice temperature change should be about four times less, i.e., the sample should heat up by $\Delta T(2 \mu\text{s}) = 26$ K and the lattice temperature T should reach about 30 K only. Thus, the 2- μ s measurement behavior provides essentially nonequilibrium conditions for 2D electrons: $T_e/T = 7.4$. The analysis of the photoresponse oscillograms showed that essentially nonequilibrium conditions are realized for periodic 2- μ s pulses at 10 Hz repetition frequency in the entire operating range of electric fields from 50 to 450 V/cm in which the ratio T_e/T takes values 6.6–8.4. When using single field pulses and increasing their amplitude to 2300 V/cm, this ratio monotonously decreases to 4.

Finally, we examined the THz electroluminescence spectra obtained by sweeping the magnetic field in the n -InSb filter. Preliminarily, this filter was calibrated by performing the CR measurements with a quantum cascade laser operating at the frequency

of 3.25 THz. Using the characteristic function of the CR filter and deconvolution technique, the high-resolution photoresponse spectra were obtained, which were then divided by the spectral sensitivity curve of the Ge:Ga detector. Resulting dependencies of the spectral radiation density on photon energy are presented in Fig. 7 for various samples.

In the reference sample in the operating spectral range (8–24 meV), the spectral radiation density decreases monotonically with photon energy (in the limits of experimental error) at electric fields of 63–447 V/cm. This fully corresponds to the model of thermal radiation of hot 2D electrons [see Eqs. (9)–(11) in Ref. 23], which are characterized for these fields by effective temperatures $T_e = 130$ –225 K as it was shown in Fig. 5(b).

A THz emission spectrum for each grating sample additionally exhibits a resonant peak [Figs. 7(a) and 7(b)]. For the sample with 801-nm-period grating, the spectral position of the peak is almost independent of the electric field strength [Fig. 7(b)]; it coincides with the position of the fundamental 2D plasmon mode experimentally determined from the transmission measurements (11.6 meV). We attribute this peak in the emission spectrum to a radiative decay of nonequilibrium 2D plasmons with the wavevector $q = 2\pi/a$.

As follows from electrodynamic simulation of absorptivity (emissivity) spectra of the particular plasmonic structure [Fig. 1(b)], the second-order 2D plasmon resonance should be located in a spectral range of 25–30 meV and is expected to be an order of magnitude weaker than the fundamental resonance. This explains why features of a radiative decay of higher-order 2D plasmons were not observed in the emission spectra. It should be noted that the additional resonance of nonplasmonic origin, which was discussed above in the transmittance spectra (at ~ 21 meV), also did not contribute to the radiation emission. Thus, the structures under investigation demonstrated a single-line THz emission under electrical excitation.

The intensity of the observed emission peak increases with an increasing field and characterizes the effective temperature of 2D plasmons T_p . As it was mentioned above, the symmetrical part of the hot 2D electron distribution function in the AlGaIn/GaN heterostructure is well described by a Fermi–Dirac function with effective temperature T_e . Under such conditions, nonequilibrium 2D plasmons are expected to be thermally excited and the distribution function of the 2D plasmons with the energy $\hbar\omega(q)$ should be described by the Bose–Einstein function with the temperature $T_p = T_e$

$$N_q = \frac{1}{\exp(\hbar\omega(q)/k_B T_e) - 1}. \quad (3)$$

Similar consideration was successfully applied for the interpretation of experimental data on THz electroluminescence in a AlGaAs/GaAs heterostructure under 2D electron heating⁷ and on middle-infrared superradiant emission from highly doped InGaAs/AlInAs quantum wells under whole sample heating by the electric current [see Fig. 4(a) in Ref. 9]. To find out if such a consideration can be applied to the AlGaIn/GaN heterostructures studied here, we compared our experimental results on the spectral radiation density at different electric fields for the sample with 801-nm-period grating with the function $N_q(T_e)$ calculated for the

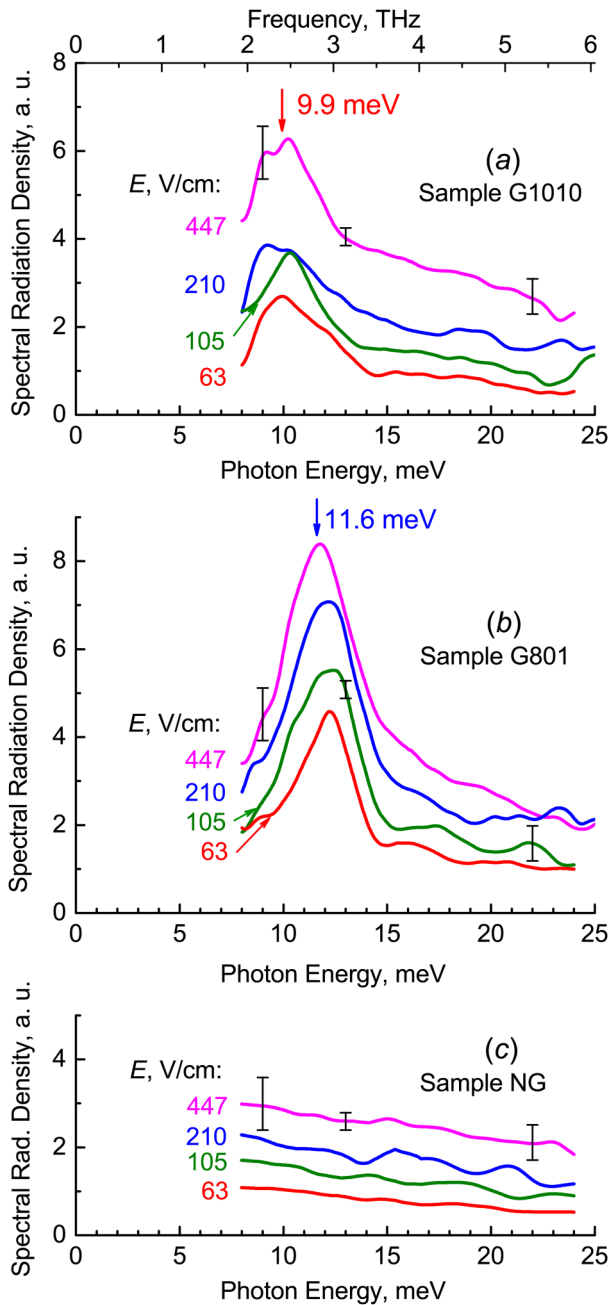


FIG. 7. THz radiation emission spectra from different samples under 2D electron heating for various values of a lateral electric field E . A n -InSb plate was used as the magnetic-field-tuned CR filter together with a Ge:Ga detector operated at 4.2 K. Spectra are shown after deconvolution with the characteristic function of the CR filter and subsequent normalization taking into account the spectral sensitivity of the detector. The same scale is used to plot the spectral density for different samples. (a) Sample with 1010-nm-period metal grating, (b) sample with 801-nm-period grating, and (c) sample without grating. Arrows in panels (a) and (b) mark the spectral positions of the fundamental 2D plasmon mode experimentally determined from the transmission measurements (see Fig. 3).

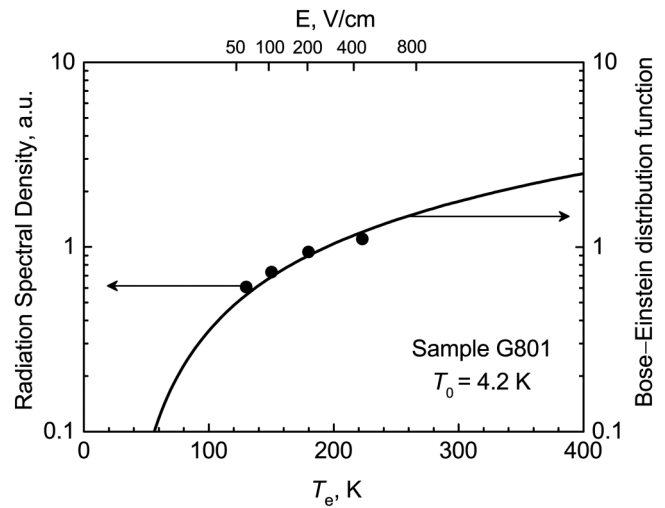


FIG. 8. Radiation spectral density at the frequency of fundamental 2D plasmon mode vs hot 2D electron temperature T_e for the sample with 801-nm-period grating. Experimental results are shown by circles. The solid line denotes the dependence expected from Bose-Einstein distribution function characterized by the temperature T_e .

2D plasmon energy $\hbar\omega(q) = 11.6$ meV. The function $N_q(T_e)$ is shown in Fig. 8 by the solid line. From the experimental spectra in Fig. 7, we took the value of the spectral radiation density at the photon energy $\hbar\omega = \hbar\omega(q)$ at every electric field E , and the corresponding experimental point was presented by a circle in Fig. 8 at a certain value of the hot 2D electron temperature T_e according to the dependence $T_e(E)$ shown in Fig. 5(b). A single scaling parameter was used to fit the whole set of the experimental points to the Bose-Einstein function. The good fitting results speak in favor of the assumption that, under electrical excitation of considered AlGaIn/GaN heterostructures, the effective temperatures of nonequilibrium 2D plasmons and hot 2D electrons are close to each other. Under these conditions, an intensive selective THz emission was observed and the amplitude of the 2D plasmon peak was 3–4 times higher than the level of thermal radiation of hot 2D electrons at the same photon energy [see Figs. 7(b) and 7(c)].

At an electric field of 447 V/cm, the power of THz emission pulse in the narrow spectral band corresponding to the 2D plasmon resonance at 11.6 meV (2.8 THz) was about 35 nW (radiation was collected in the solid angle of 0.25 srad under the sample excitation by periodic electrical pulses). The wall-plug efficiency of the THz emitter in these conditions was $\sim 1 \times 10^{-10}$. At a lower level of excitation, the wall-plug efficiency increased. For instance, at an electric field of 63 V/cm when the power of THz emission pulse was 12 nW, the wall-plug efficiency reached the value of 1.1×10^{-9} . The latter is much less than the wall-plug efficiency of a THz quantum cascade laser [$\sim 1 \times 10^{-3}$ at a frequency of 2.7 THz and temperature of 20 K (see Ref. 26)]; nevertheless, the considered THz emitter can find applications due to its simplicity (and low price) and the opportunity to control the operating

frequency by the grating period. The same epitaxial structure (same 2DEG and contact layers) can be used to fabricate THz emitters operating at various frequencies by giving different parameters to the EBL equipment. The THz radiation power can be enhanced by scaling the device area and/or by increasing the applied voltage. It should be noted that the present work is one of the first studies of THz emission due to 2D plasmons in nitride-based nanostructures (see also Ref. 16). Intensive narrowband THz radiation associated with a radiative decay of nonequilibrium 2D plasmons has been experimentally observed for the first time.

The emission peak obtained for the sample with 1010-nm-period grating [Fig. 7(a)] also can be associated with the fundamental 2D plasmon mode (9.9 meV in this sample). Unfortunately, the THz emission spectra for this sample have a lower signal-to-noise ratio that is caused by a rather low Ge:Ga detector sensitivity in the vicinity of 9.9 meV (about 20% of the maximum value at 13 meV). Due to this reason, there are some distortions of the spectra at photon energies less than 10.5 meV and, in particular, fluctuations of the peak position. Nevertheless, it is possible to distinguish a low-frequency shift of the whole emission peak (~ 2 meV) with increasing the grating period from 801 to 1010 nm, which is in good agreement with the transmission spectra.

VII. CONCLUSION

In conclusion, electrically excited 2D plasmons have been studied in the AlGaIn/GaN heterostructure under essentially nonequilibrium conditions when the effective temperature of 2D plasmons is much higher than the lattice temperature (about 7–8 times). The electroluminescence studies performed on the samples with surface metal grating have revealed a significant (about 3–4 times) selective amplification of THz radiation emission in the vicinity of 2D plasmon resonance in comparison with the level of blackbodylike thermal emission of hot 2D electrons. This amplification has been associated with a radiative decay of nonequilibrium 2D plasmons. Different grating periods have been examined and the possibility of fabricating narrowband terahertz emitters in which operating frequency is controlled by the grating period has been experimentally proved for the AlGaIn/GaN platform. The exact spectral position of the fundamental 2D plasmon mode has been preliminarily determined for each sample from the equilibrium transmission measurements at various temperatures. The transmittance and absorptivity/emissivity spectra have also been theoretically simulated using a rigorous solution of Maxwell's equations. The simulated spectra are in satisfactory agreement with the experimental data on THz radiation transmission and emission.

The field dependencies of the effective temperature of hot 2D electrons have been determined by means of I - V characteristics and their analysis using the power balance equation. The THz electroluminescence studies have been performed using short voltage pulses (2 μ s) and the fast Ge:Ga detector. A method has been developed for determining the degree of sample lattice heating under pulsed electrical excitation. The method is based on the analysis of the integral photoresponse oscillograms. Using this method, the technique for spectral measurements of THz electroluminescence has been optimized to provide the essentially nonequilibrium conditions and maximum signal/noise ratio. An analysis of the THz

emission spectra has shown that for a given electric field, the effective temperature of nonequilibrium 2D plasmons is close to the hot 2D electron temperature.

The results of the work may have applications in GaN-based portable sources of terahertz radiation operating under electrical pumping.

SUPPLEMENTARY MATERIAL

See the [supplementary material](#) for the detailed description of the contact and grating fabrication and for some aspects of the optical transmission measurements.

ACKNOWLEDGMENTS

We thank V. I. Gavrilenko, A. V. Antonov, A. A. Toropov, and A. N. Poddubny for helpful discussions, and Mathias Meschke for advice on the electron beam lithography process. Financial supports from the Russian Foundation for Basic Research (Grant No. 18-02-00848) and the Ministry of Science and Higher Education of the Russian Federation (State Assignment No. 3.933.2017/4.6) are gratefully acknowledged.

REFERENCES

- ¹N. Dyakonova, F. Teppe, J. Łusakowski, W. Knap, M. Levenshtein, A. Dmitriev, M. Shur, S. Bollaert, and A. Cappy, *J. Appl. Phys.* **97**, 114313 (2005).
- ²T. Otsuji, Y. Meziani, T. Nishimura, T. Suemitsu, W. Knap, E. Sano, T. Asano, and V. Popov, *J. Phys. Condens. Matter* **20**, 384206 (2008).
- ³M. Dyakonov and M. Shur, *Phys. Rev. Lett.* **71**, 2465 (1993).
- ⁴D. Fateev, V. Popov, and M. Shur, *Semiconductors* **44**, 1406–1413 (2010).
- ⁵D. Tsui, E. Gornik, and R. Logan, *Solid State Commun.* **35**, 875–877 (1980).
- ⁶N. Okisu, Y. Sambe, and T. Kobayashi, *Appl. Phys. Lett.* **48**, 776–778 (1986).
- ⁷K. Hirakawa, K. Yamanaka, M. Grayson, and D. Tsui, *Appl. Phys. Lett.* **67**, 2326–2328 (1995).
- ⁸T. Laurent, Y. Todorov, A. Vasanelli, A. Delteil, C. Sirtori, I. Sagnes, and G. Beaudoin, *Phys. Rev. Lett.* **115**, 187402 (2015).
- ⁹T. Laurent, Y. Todorov, A. Vasanelli, I. Sagnes, G. Beaudoin, and C. Sirtori, *Appl. Phys. Lett.* **107**, 241112 (2015).
- ¹⁰B. Askenazi, A. Vasanelli, Y. Todorov, E. Sakat, J.-J. Greffet, G. Beaudoin, I. Sagnes, and C. Sirtori, *ACS Photonics* **4**, 2550–2555 (2017).
- ¹¹J.-Y. Lu, L.-J. Chen, T.-F. Kao, H.-H. Chang, H.-W. Chen, A.-S. Liu, Y.-C. Chen, R.-B. Wu, W.-S. Liu, J.-I. Chyi *et al.*, *IEEE Photonics Technol. Lett.* **18**, 2254–2256 (2006).
- ¹²V. Wallace, A. Fitzgerald, S. Shankar, N. Flanagan, R. Pye, J. Cluff, and D. Arnone, *Br. J. Dermatol.* **151**, 424–432 (2004).
- ¹³A. Muravjov, D. Veksler, V. Popov, O. Polischuk, N. Pala, X. Hu, R. Gaska, H. Saxena, R. Peale, and M. Shur, *Appl. Phys. Lett.* **96**, 042105 (2010).
- ¹⁴L. Wang, X.-S. Chen, W.-D. Hu, and W. Lu, *IEEE J. Sel. Top. Quantum Electron.* **19**, 8400507 (2012).
- ¹⁵H. Spisser, A.-S. Grimault-Jacquín, N. Zerounian, A. Aassime, L. Cao, F. Boone, H. Maher, Y. Cordier, and F. Aniel, *J. Infrared Millim. Terahertz Waves* **37**, 243–257 (2016).
- ¹⁶V. Jakštas, I. Grigelionis, V. Janonis, G. Valušis, I. Kašalynas, G. Seniutinas, S. Juodkazis, P. Prystawko, and M. Leszczyński, *Appl. Phys. Lett.* **110**, 202101 (2017).
- ¹⁷M. Y. Vinnichenko, V. Shalygin, M. Moldavskaya, A. Artemyev, G. A. Melentev, L. E. Vorobjev, D. Firsov, V. Korotyeyev, A. Sakharov, E. Zavarin *et al.*, *J. Phys. Conf. Ser.* **1199**, 012014 (2019).
- ¹⁸Y. M. Lyaschuk and V. Korotyeyev, *Ukr. J. Phys.* **62**, 889 (2017).
- ¹⁹O. Matov, O. Meshkov, and V. Popov, *J. Exp. Theoret. Phys.* **86**, 538–544 (1998).

²⁰V. V. Popov, *J. Infrared Millim. Terahertz Waves* **32**, 1178 (2011).

²¹W. B. Cook and S. Perkowitz, *Appl. Opt.* **24**, 1773–1775 (1985).

²²A. Tsatsulnikov, V. Lundin, E. Zavarin, M. Yagovkina, A. Sakharov, S. Usov, V. Zemlyakov, V. Egorkin, K. Bulashevich, S. Y. Karpov *et al.*, *Semiconductors* **50**, 1383–1389 (2016).

²³V. Shalygin, L. Vorobjev, D. Firsov, A. Sofronov, G. Melentyev, W. Lundin, A. Nikolaev, A. Sakharov, and A. Tsatsulnikov, *J. Appl. Phys.* **109**, 073108 (2011).

²⁴V. Shalygin, L. Vorobjev, D. Firsov, A. Sofronov, G. Melentyev, M. Y. Vinnichenko, V. Lundin, A. Nikolaev, A. Sakharov, and A. Tsatsulnikov, *Bull. Russ. Acad. Sci. Phys.* **76**, 207–210 (2012).

²⁵V. Shalygin, L. Vorobjev, D. Firsov, A. Sofronov, G. Melentyev, W. Lundin, A. Sakharov, and A. Tsatsulnikov, *AIP Conf. Proc.* **1566**, 449–450 (2013).

²⁶C. Yu, H. Zhu, F. Wang, G. Chang, H. Zhu, J. Chen, P. Chen, Z. Tang, W. Lu, C. Shen *et al.*, *Appl. Phys. Lett.* **113**, 121114 (2018).